Vietnam Journal of Earth Sciences, 48(2), 309−332, https://doi.org/10.15625/2615-9783/24217

Vietnam Journal of Earth Sciences
https://vjs.ac.vn/index.php/jse

Geochronology, geochemistry, and associated tectonics of Permian-Triassic magmas in NW Truong Son Fold Belt

Tran Trong Hoa[1], Usuki Tadashi[2], Tran Tuan-Anh[1], Lan Ching-Ying[3], Nguyen Hoang[1,*], Vu Hoang Ly[1], Pham Thi Dung[1], Pham Ngoc Can[1], Tran Thi Huong[1], Duangpaseuth Somsanith[4], Soulintone Oneta[4], Phan Duc Le[5,6]

[1]*Institute of Earth Sciences, Vietnam Academy of Science and Technology, Hanoi, Vietnam*
[2]*Department of Geosciences, National Taiwan University, Taiwan*
[3]*Institute of Earth Sciences, Academia Sinica, Taiwan*
[4]*Department of Earth Science, Laos National Authority for Science and Technology, PDR Laos*
[5]*Vietnam Institute of Geosciences and Mineral Resources, Ministry of Agriculture and Environment, Vietnam*
[6]*Graduate University of Science and Technology, VAST, Hanoi, Vietnam*

Received 30 September 2025; Received in revised form 22 January 2026; Accepted 13 February 2026

ABSTRACT

The Permian-Triassic igneous rocks of the Truong Son Fold Belt, on the northeastern margin of the Indochina block, formed during Paleotethyan subduction and the subsequent collision with the South China block. Systematic variations in zircon ages, geochemistry, and isotopic compositions are observed from northern Laos toward the Song Ma Suture zone, the collisional boundary with the South China block. In the Xiang Khuang-Muang Khoun (MK) area, 170–200 km from the suture, magmatic rocks (271–253 Ma) include gabbros and I-type granitoids with relatively higher εNd(t) values (-1.5 to -9) and lower $^{87}Sr/^{86}Sr_i$ (0.704–0.717). Toward the suture, in the Nam Phao-Kim Cuong area, granitoids dated at 260–251 Ma are predominantly S-type, highly peraluminous granites with intermediate isotopic εNd_i values (-7.4 to -9) and $^{87}Sr/^{86}Sr_i$ values (0.7115–0.7285). In the Sam Neua (SN) area, closest to the suture, granitoids dated at 251–244 Ma are primarily I-type and minorly S-type, with highly enriched isotopic compositions (εNd_i of -8.4 to -14; $^{87}Sr/^{86}Sr_i$ between 0.708 and 0.775). The trace-element chemistry of all granitoids indicates volcanic-arc affinities, though signatures also suggest intraplate and post-collisional influences. The association of granitoids with coeval gabbro-diorites in the MK area suggests binary mixing between mantle magmas and Mesoproterozoic crust-derived melts. In contrast, felsic magmas in the SN area likely reflect melting of diverse crustal components, including Paleoproterozoic continental crust of South China affinity. The suture zone-ward younging of magmatism is consistent with slab rollback during the final stages of continental collision.

Keywords: Paleotethys subduction, post-collision granitoids, Song Ma Suture, Truong Son Fold belt, Permian-Triassic granitoids.

1. Introduction

Indochina, one of the major continental blocks in Southeast Asia, is bounded by major Paleotethyan suture zones to the north (Jinshajiang-Ailaoshan-Song Ma) and to the southwest (Jin Hong Nang-Sakaeo). This makes it a key region for interpreting the closure of the Paleotethys and its amalgamation with surrounding terranes (Metcalfe, 2013) (Fig. 1).

*Corresponding author, Email: nghoang@ies.vast.vn

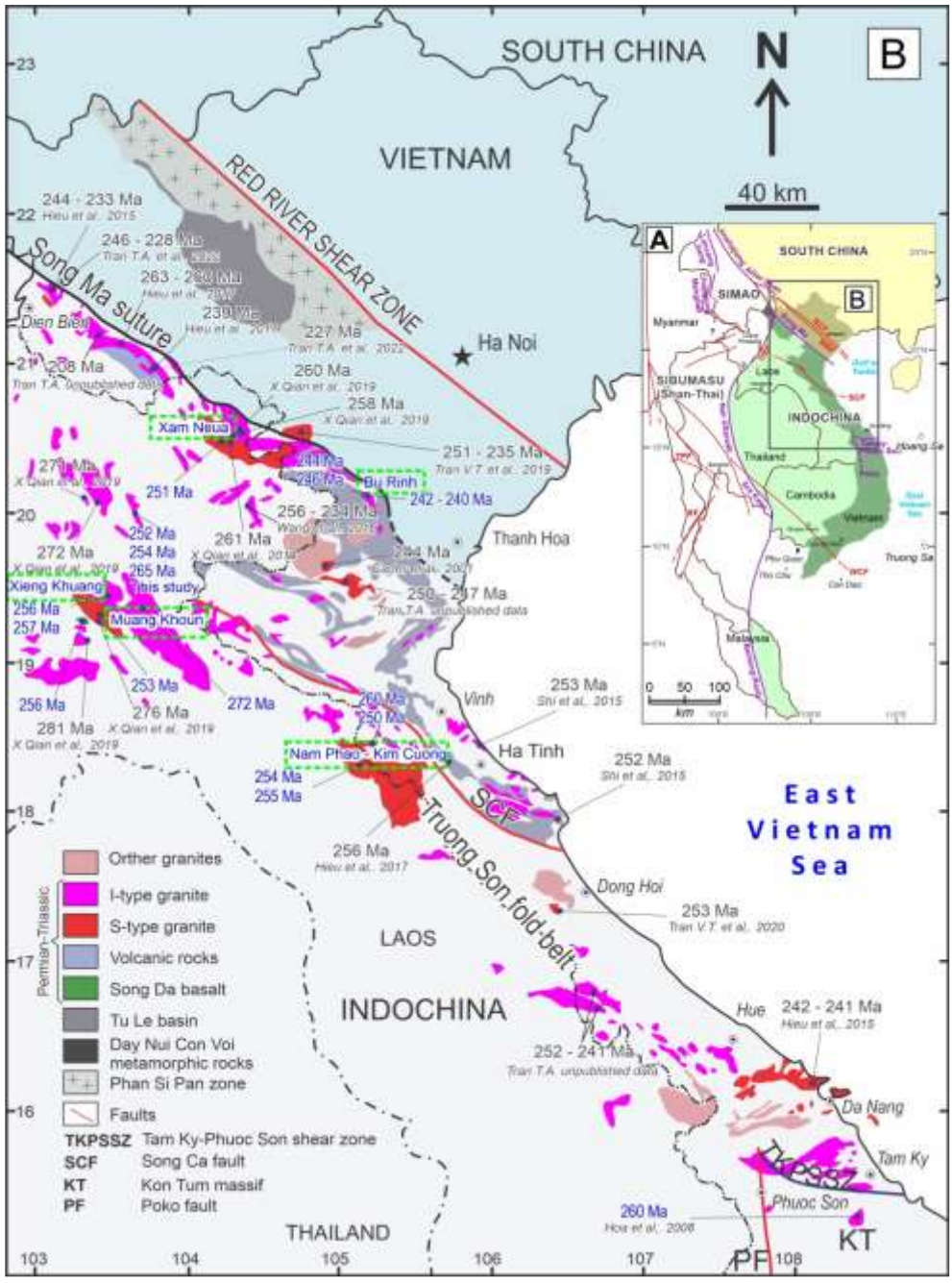

Figure 1. Simplified map of distribution of granitoids in the TSFB (A) Study area in regional tectonic structures; (B) Rock sampling locations in Sam (Xam) Neua (SN), Nam Phao (NP), Kim Cuong (KC), Xieng Khuang (XK), and Muong Khoun MK) areas. Numbers are age data from the literature (black) and this study (blue). Modified from Phan (2009)

The Truong Son Fold Belt (TSFB), extending over 100 kilometers across Laos and Vietnam, forms the Indochina block's northeastern margin. It developed through

subduction along the northern Paleotethyan margin and subsequent collision with the South China block (Tran et al., 2008; Liu et al., 2012; Usuki et al., 2013; Qian et al., 2019; Hou et al., 2019). Late Carboniferous to Triassic magmas related to the Indochina orogeny are widespread in the TSFB and preserve evidence of oceanic subduction (Jian et al., 2008; Kamvong et al., 2014), collision, as well as post-collisional magmatism (Lan et al., 2000; Tran et al., 2008; Liu et al., 2012; Qian et al., 2019).

Lan et al. (2000) first noted that I-type granitoids in the Dien Bien formation, in the northernmost TSFB, were generated by subduction under the Indochina margin (see Tran et al., 2024). Later, Tran et al. (2008) summarized the geochemical features of Permian-Triassic felsic magmas across the TSFB and divided the magmatism into subduction-, syn-collision-, and post-collision-stage magmatism. Based on U-Pb isotopic ages, Liu et al. (2012) refined this sequence into three stages: 280–245 Ma, 245–230 Ma, and 230–200 Ma. Comparable studies of Permian-Triassic felsic magmatism have also been carried out in the northern Laos section of the TSFB (Wang et al., 2016; Qian et al., 2019).

In Vietnam, the TSFB is disrupted by numerous northwest-orienting shear zones, which complicate the reconstruction of its original magmatic arc structures (Lepvrier et al., 1997). In contrast, the Lao segment is less affected by shearing, making it better suited for investigating the tectono-magmatic processes associated with Paleotethyan subduction.

This study presents U-Pb ages, magma geochemistry, and strontium-neodymium isotope data for Permian to Early Triassic magmatic rocks from Laos and Vietnam, northwestern and western TSFB, respectively. Our objectives are to define the main geochemical and isotopic characteristics of magmatism across different tectonic stages; (2) constrain the magma sources; and (3) clarify the Indochina block's geodynamic setting in the Permian-Triassic.

2. Geology

The Truong Son Fold Belt (TSFB) is approximately 50–100 km wide and extends over more than 1,000 km across northwest Vietnam, northeast Laos, and the Vietnam-Laos border. Its northwestern part is cut by the sub-meridional Loei belt (Tran-Van et al., 2020). The TSFB's northern boundary is marked by the Song Ma fault that separates it from the Song Ma suture zone (Tran-Van, 1977; Le et al., 1982; Lepvrier et al., 2008; Phan et al., 2009; Tran-Van and Vu, 2011).

The study area consists mainly of Early-Middle Paleozoic and Middle-Late Paleozoic to Early Mesozoic sedimentary, metamorphic, and magmatic rocks, with Permian-Triassic intermediate to felsic intrusions being dominant (Fig. 1). In Laos, Neoproterozoic-Cambrian metamorphic rocks, including gneiss, mica schist, and amphibolite, occur in three narrow belts, separated by Mesozoic sedimentary sequences of terrigenous, terrigenous-carbonate, and volcaniclastic rocks (Fig. 1). Proterozoic metamorphic suites are exposed in the Nong Het area, east of Xiang (Xieng) Khuang province near the Thanh Hoa province border in Vietnam. In eastern Huaphan province (Sam Neua region), the Sop Bao area shows a similar geological context to the central part of the western Song Ma suture zone, where Neoproterozoic and Early Paleozoic sedimentary-metamorphic rocks, serpentinite, and scattered metabasalt, metadolerite, diorite, and plagiogranite are widespread (e.g., Zhang et al., 2020) (Fig. 1).

The Permian-Triassic magmatic rocks of the study area are primarily composed of hornblende- and biotite granite, granodiorite, and minor occurrences of gabbro and quartz diorite. Hornblende granites form intrusions ranging from a few tens to several hundred square kilometers, widely distributed in

Muang Khoun (MK), Xiang Khuang (XK), and northeast of Sam Neua (SN) (Figs. 1 & 2a-A, -B, -C). Biotite granites occur in the SN, MK, and Nam Phao (NP) areas (Fig. 2a-D, -E, -F) as stocks or batholiths several hundred km² in size. In the SN and MK areas, some biotite granites contain muscovite or garnet. Gabbro and quartz diorite appear as enclaves within granitoids in the MK area, and fine-grained gabbro also forms minor intrusions in Devonian metasediments near a biotite granite body (Fig. 2a-A, -B).

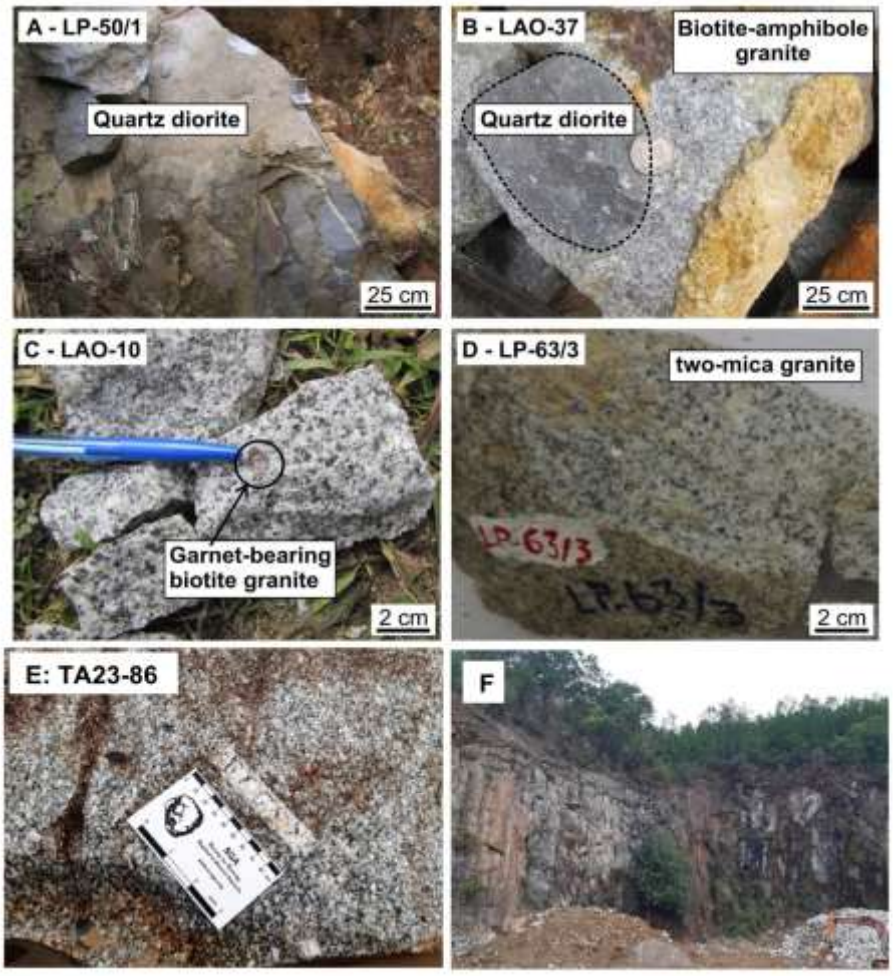

Figure 2a. (A) Outcrop of quartz diorite (LP-50/1) among Paleozoic metamorphic rocks, MK area; (B) Enclaves of quartz diorite (LAO-37) in hornblende granite (LAO-37A) in Muong Khoun; (C) Biotite granite containing garnet in sample LAO-10, SN area; (D) Two-mica granite in NP area, sample LP-63/3; (E) Outcrop of two-mica granite in Kim Cuong; (F) Granite quarry in the Kim Cuong area

In the SN area, volcanic rocks such as rhyodacite and rhyolite are present and widespread in the Anisian (Middle Triassic) volcanoclastic deposits of the SN basin (Tran et al., 2019). These are closely associated with hornblende granites. In the XK area, porphyritic dacite occurs together with granodiorite and hornblende granite (Fig. 1).

3. Petrography

Granitoid samples were collected from northern Laos, including Muang Khoun

(MK), Xiang Khuang (XK), Sam Neua (SN), and Nam Phao (NP), as well as from Kim Cuong (KC) in western Vietnam, which is the continuation of the Nam Phao block (Fig. 1). Below is a summary of their main petrographic features.

Granodiorite: Samples from MK (e.g., LP-50/1, LP-50/2-1), XK (e.g., LAO-2), and SN (e.g., LAO-10) are fine- to medium-grained with sub-euhedral textures. These magmas are comprised mainly of K-feldspar, plagioclase, hornblende, biotite, and quartz, with apatite, titanite, and zircon as accessory minerals (Fig. 2b-A, -B). Biotite and hornblende are typically brownish-green to green in color and often exhibit chloritization and partial epidotization.

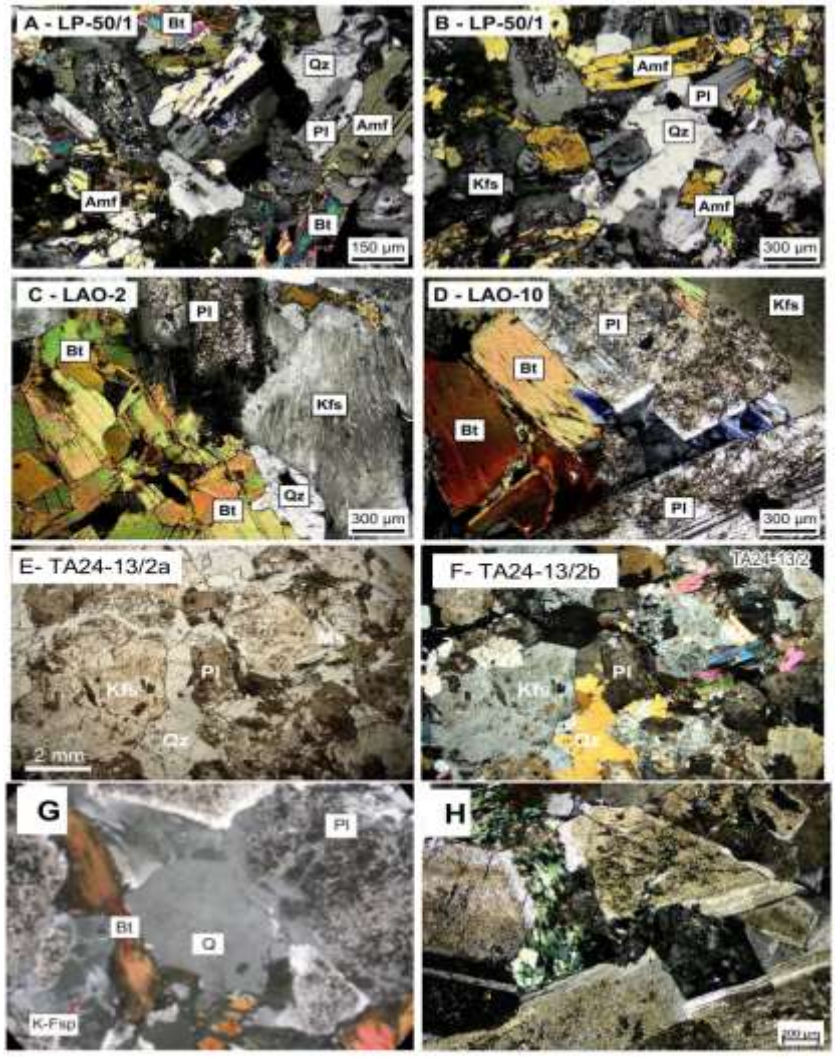

Figure 2b. Microphotographs of (A) Quartz diorite, LP-50/1 and (B) Granodiorite, LP-50/1-2 in the MK area; (C) Biotite granite, LAO-2, XK area; (D) Garnet-bearing biotite granite, LAO-10, SN area; (E) Two-mica granite, TA24-13/2a (plain light), NP area; (F) Two-mica, TA24-13/2b (polarized light); (G) Two-mica granite under plain light, sample TA23-86, Kim Cuong area; (H) Two-mica granite, under polarized light, sample TA23-87, Kim Cuong area. The abbreviations Q: Quartz; Kfs: K-feldspar; Pl: Plagioclase; Bi: Biotite; Amp: Amphibole; and Cpx: clinopyroxene

Hornblende granite: Samples from XK (LAO-2, LAO-3, LAO-4) (Fig. 2b-C) and MK (LAO-29, LAO-37A, LAO-38, LAO-40) have similar mineral assemblages to granodiorite but contain higher proportions of feldspar.

Biotite granite: Samples from MK (e.g., LAO-41, LAO-43A) and SN (e.g., LAO-9, LAO-10, LAO-11A-B, LAO-15, LAO-17) (Fig. 2b-D) share a mineral assemblage with hornblende granite but lack hornblende. Some contain garnet, sillimanite, and muscovite.

Two-mica granite: Samples from NP (e.g., LP-63/1, LAO-1D) and KC (e.g., TA24-13/2) are medium- to coarse-grained, and subhedral to anhedral textured. The magmas are comprised of muscovite, biotite, K-feldspar, plagioclase, and quartz, with apatite, zircon, titanite, and hornblende as accessory minerals (Figs. 2b-E, -F, -G, -H).

4. Analytical procedures

4.1. U-Pb age dating and Hf isotope measurements

Zircon crystals were extracted from ~1 kg magmatic rocks using magnetic and heavy liquid methods, followed by hand-picking under a binocular microscope. Their internal structures and inclusions were examined using transmitted/reflected light microscopy, and cathodoluminescence (CL) imaging with a Gatan Mini-CL attached to a JEOL JSM-6360LV SEM at Academia Sinica (Taipei). Selected grains were mounted in epoxy and polished to half-thickness for in-situ analyses.

Zircon U-Pb dating analysis was performed at NTU-Geosciences using an Agilent 7500s LA-ICP-MS with a New Wave UP213 laser (30 μm spot size). GLITTER 4.0 software and GJ-1 zircon, the external standard (608.5 ± 0.4 Ma; Jackson et al., 2004), were used to refine the data. Reference zircons 91500 and Plešovice were periodically measured and yielded ages within the recommended range, respectively: 1062.2 ± 5.1 Ma (Wiedenbeck et al., 1995) and 339.4 ± 2.9 Ma (Sláma et al., 2008). Standard Pb correction followed Andersen (2002). ISOPLOT 4 (Ludwig, 2008) was used to construct the Concordia and age-probability plots. Because young zircons produce little ^{207}Pb, pooled $^{206}Pb/^{238}U$ ages were used to represent crystallization ages, reported at 2σ (95% confidence).

Lu-Hf isotopic analyses were performed at Academia Sinica employing a Nu Plasma HR MC-ICP-MS coupled with a Photon Machines Analyte G2 excimer laser. Analyses were performed on the same zircon crystals used for U-Pb dating, with a ~40 μm spots, 26 seconds of ablation time, an 8 Hz repetition rate, and 100 mJ of energy. The Mud Tank zircon was used as a secondary standard, yielding a $^{176}Hf/^{177}Hf$ ratio of 0.282530 ± 0.0050 (2σ, n = 63), consistent with published values (Woodhead and Hergt, 2005). Model ages and $\varepsilon Hf_{(t)}$ values were calculated using the ^{176}Lu decay constant of 1.867×10^{-11} yr^{-1} (Scherer et al., 2001). Full zircon U-Pb and Lu-Hf data are given in Supplementary A (*).

4.2. Major and trace element analysis

About 100 g of fresh, crushed samples were cleaned ultrasonically in deionized water, dried, and ground in an agate mill. Major elements were determined by X-ray fluorescence (XRF) on fused glass beads at Akita University, Japan, using a Rigaku Mini-Z Analyzer. For trace elements and isotopes, powders (~200 mg) were digested using mixtures of concentrated $HClO_4$ (11 M), HF (26 M), and HNO_3 (15 M). The acids were mixed in equal volume (1:1:1 mL) in 15-mL Savillex beakers, and heated on a hotplate at 135 degrees for at least 72 hours. The solution was then refluxed with 1 mL of 15 M HNO_3, evaporated, and re-dissolved in 3 M HNO_3. A small aliquot (~10%) was diluted to 0.5 M HNO_3 for trace element analysis at Akita University, using a quadrupole (Q)-ICP-MS (Agilent 7500s). The remaining solution was

reserved for Sr and Nd isotope separation. During the ICP-MS analysis, reference materials JB-3, JA-2, JGb-1, JG-2, JG-3, and JR-3 were used for calibration and as external references to assess analytical accuracy. Analytical uncertainties are between 0.5 and 3% for major elements and between 1 and 10% for trace elements. Detailed procedures follow those described by Fukuyama et al. (2013, 2017).

Trace elements with uncertainties above 10% and up to 20% were re-analyzed. These include Rb, Sr, Nb, Zr, and Y. They were measured by XRF from pressed pellets at the Institute of Earth Sciences (former Institute of Geological Sciences, VAST), using Bruker Pioneer XRF mass spectrometer to verify data precision and accuracy (Le et al., 2017).

Major and trace element data are reported in Table 1.

4.3. Whole-rock Sr and Nd isotope analysis

Strontium and neodymium isotope separation was carried out using cation exchange resins (Bio-Rad AG 50W-X8 for Sr; Eichrom Ln resin for Nd). Isotopic ratios were acquired at Academia Sinica using Finnigan MAT 262 and TRITON mass spectrometers, with a double-Re-filament configuration. Mass fractionation was normalized to $^{86}Sr/^{88}Sr = 0.1194$ and $^{146}Nd/^{144}Nd = 0.7219$. Standards yielded $^{86}Sr/^{87}Sr = 0.710247 \pm 0.000026$ (NBS987; n= 25) and $^{143}Nd/^{144}Nd = 0.511814 \pm 0.000009$ (La Jolla; n= 25), within accepted values. Procedural blanks were ~210 pg Sr and ~120 pg Nd. Within-run precision (2σ) was better than ±0.000010. Details of chemical and analytical procedures follow Jahn et al. (2009). The Sr-Nd isotopic data are reported in Supplementary B (*).

Table 1. Geochemical and isotopic compositions of Permian-Triassic granitoitds in the Truong Son Fold Belt

Sample	**LAO-9**	**LAO-10**	**LAO-11A**	**LAO-11B**	**LP-63/1**	**LP-63/2**
Location	Sam Nuea	Sam Nuea	Sam Nuea	Sam Nuea	Nam Phao	Nam Phao
Rock type	S-type	S-type	S-type	S-type	S-type	S-type
	Bt granite	Grt-Bt granite	Bt granite	Bt granite	Bt granite	Bt granite
Age (mill. y)		251			255	254
SiO_2	72.88	65.57	68.28	74.26	67.22	67.61
TiO_2	0.27	0.80	0.48	0.20	0.67	0.6
Al_2O_3	14.57	15.45	13.72	13.43	14.82	14.83
Fe_2O_3	2.12	5.46	4.71	0.76	4.06	3.85
MnO	0.03	0.08	0.09	0.01	0.04	0.04
MgO	0.65	2.27	2.84	0.26	2.41	2.22
CaO	0.61	2.99	3.83	0.37	2.47	2.29
Na_2O	2.60	2.29	1.11	1.73	2.01	2.02
K_2O	5.11	3.96	2.75	8.65	5.03	5.01
P_2O_5	0.12	0.22	0.12	0.12	0.12	0.12
LOI	1.69	1.39	2.77	0.75	0.93	0.83
Total	100.65	100.48	100.70	100.55	99.8	99.42
Rb*	213.0	169.4	141.4	383.0	267.0	248.0
Sr*	105.0	272.0	95.0	80.0	221.0	208.0
Ba	753.0	954.0	325.0	307.0	860.0	890.0
Zr*	177.0	241.0	176.0	63.0	269.0	256.0
Hf	5.0	7.5	5.5	1.1	0.7	0.4
Nb	8.2	22.7	12.8	9.6	15.9	12.0
Ta	1.0	2.5	1.4	1.4	0.9	1.4
Sc	5.0	13.0	10.0	7.0	8.7	6.6
Y*	21.9	28.3	22.9	12.1	14.0	14.8
La	40.0	58.9	30.0	12.5	61.7	22.4
Ce	78.5	114.5	58.6	24.7	125.7	44.4

Pr	8.9	13.1	6.6	2.8	14.1	5.1
Nd	31.2	46.2	23.7	10.5	50.2	18.4
Sm	6.4	8.3	4.4	2.5	9.3	4.0
Eu	1.0	1.5	0.8	0.5	1.5	0.8
Gd	5.7	6.9	3.9	2.5	7.9	3.7
Tb	0.8	0.9	0.6	0.4	0.9	0.5
Dy	4.3	4.9	3.3	2.2	3.5	2.8
Ho	0.8	0.9	0.7	0.4	0.5	0.5
Er	1.9	2.5	1.9	1.2	1.1	1.3
Tm	0.3	0.4	0.3	0.2	0.1	0.2
Yb	1.8	2.4	2.0	1.0	0.7	1.3
Lu	0.3	0.4	0.3	0.1	0.1	0.2
V	25.0	94.0	61.0	3.5	52.0	21.3
Cr	21.0	63.0	70.0	32.3	37.7	11.8
Co	3.6	10.9	10.7	1.3	7.8	3.2
Ni	6.0	17.0	24.0	1.4	13.4	5.8
Cu	18.0	14.0	10.0	75.9	-	-
Zn	23.0	71.0	67.0	9.9	-	-
Pb	28.0	27.0	21.0	40.7	24.1	27.7
Ga	17.1	19.0	18.9	15.0	-	-
Th	24.2	28.1	9.8	6.3	32.4	10.5
U	6.6	5.7	4.4	4.6	2.1	4.8
$^{87}Sr/^{86}Sr$	0.744392	0.723915	0.741738	0.778260	0.724139	0.731183
±2s	0.000010	0.000009	0.000008	0.000010	0.000009	0.000010
$^{143}Nd/^{144}Nd$	0.511946	0.511930	0.511783	0.511855	0.512043	0.512075
±2σ	0.000008	0.000009	0.000008	0.000010	0.000010	0.000008
$^{87}Rb/^{86}Sr$	5.660	1.738	4.153	13.357	3.371	3.327
$^{87}Sr/^{86}Sr(t)$	0.741712	0.721309	0.739068	0.775458	0.721532	0.728551
$^{147}Sm/^{144}Nd$	0.12549	0.11100	0.11530	0.14659	0.11425	0.13301
$^{143}Nd/^{144}Nd(t)$	0.51174	0.51175	0.51159	0.51161	0.51185	0.51185
εNd(0)	-13.5	-13.8	-16.7	-15.3	-11.6	-11.0
εNd(t)	-11.3	-11.1	-14.1	-13.7	-9.0	-9.0
T_{DM}	2.1.E+09	1.8.E+09	2.1.E+09	2.9.E+09	1.7.E+09	2.0.E+09

Sample	**TA23-75/2**	**TA23-86**	**TA23-87**	**TA23-88/2**	**TA24-13/2**	**TA24-13/3**	**TA24-13/5**
Location	Thanh Hoa	Kim Cuong	Kim Cuong	Kim Cuong	Kim Cuong	Kim Cuong	Kim Cuong
Rock type	I-type	S-type	S-type	S-type	S-type	S-type	S-type
	Bt granite	2-mica granite	2-mica granite	2-mica granite	2-mica granite	2-mica granite	2-mica granite
Age (mill. y)	242	249			260	260	
SiO_2	74.52	70.94	67.99	71.41	70.75	62.20	71.91
TiO_2	0.10	0.30	0.39	0.14	0.22	0.80	0.13
Al_2O_3	13.33	14.71	15.60	13.94	14.39	16.41	14.47
Fe_2O_3	2.02	2.87	4.06	1.77	3.20	6.50	1.95
MnO	0.03	0.06	0.07	0.05	0.07	0.07	0.04
MgO	0.16	0.71	0.97	0.52	0.63	1.98	0.35
CaO	1.13	1.79	3.03	1.24	1.64	4.18	0.82
Na_2O	3.81	2.92	3.25	3.78	3.02	2.77	3.24
K_2O	4.20	4.26	3.52	4.44	3.68	2.87	4.87
P_2O_5	0.02	0.16	0.14	0.06	0.11	0.26	0.25
LOI	0.65	0.81	0.91	1.71	1.31	1.79	1.20
Total	99.97	99.52	99.92	99.05	99.03	99.81	99.24
Rb*	191.1	225.0	157.0	229.0	145.0	131.0	305.0
Sr*	61.2	180.0	300.0	110.0	240.0	420.0	60.0
Ba	455.9	520.0	670.0	140.0	540.0	1080.0	180.0

Zr*	98.0	107.6	172.5	56.3	-	-	-
Hf	3.9	-	-	-	-	-	-
Nb	7.7	11.0	11.0	8.0	12.0	13.0	10.0
Ta	1.1	1.6	1.1	1.5	0.9	0.5	1.6
Sc	-	-	-	-	-	-	-
Y*	41.5	23.2	26.1	34.7	36.7	22.7	17.0
La	25.6	28.9	44.3	17.2	35.4	52.2	10.9
Ce	49.7	53.6	86.8	36.2	70.4	108.0	21.5
Pr	5.7	6.9	10.7	4.6	9.3	12.0	2.5
Nd	22.3	23.1	39.0	16.8	31.9	44.2	8.9
Sm	5.2	4.5	6.6	3.5	7.3	8.7	2.4
Eu	0.3	1.0	1.4	0.4	1.4	2.1	0.4
Gd	5.3	3.5	6.0	4.4	6.3	7.0	2.8
Tb	1.0	0.6	0.8	0.8	1.1	1.0	0.5
Dy	6.3	4.0	4.4	5.3	6.6	5.2	3.2
Ho	1.4	0.7	0.9	1.1	1.4	0.9	0.5
Er	4.4	1.9	2.4	3.5	3.7	2.2	1.3
Tm	0.7	0.3	0.4	0.5	0.6	0.4	0.2
Yb	4.8	2.6	2.0	3.7	3.5	2.2	1.1
Lu	0.7	0.4	0.3	0.6	0.5	0.3	0.2
V	2.9	28.0	36.0	15.0	-	10.0	-
Cr	7.4	0.0	0.0	0.0	0.0	0.0	0.0
Co	1.1	4.2	5.2	1.6	4.4	11.1	2.3
Ni	4.4	9.0	11.0	11.0	119.0	48.0	27.0
Cu	15.4	20.0	-	-	-	20.0	-
Zn	33.6	48.0	51.0	23.0	49.0	104.0	108.0
Pb	30.6	39.0	26.0	38.0	33.0	42.0	48.0
Ga		17.0	19.0	17.0	17.0	19.0	16.0
Th	21.1	12.5	13.8	7.2	11.6	13.0	2.6
U	6.3	5.0	8.0	10.0	3.0	1.5	8.0
$^{87}Sr/^{86}Sr$	0.755642	0.725815	0.714076				
±2s	0.000009	0.000009	0.000009				
$^{143}Nd/^{144}Nd$	0.512124	0.512093	0.512112				
±2σ	0.000012	0.000014	0.000012				
$^{87}Rb/^{86}Sr$	8.719	3.488	1.460				
$^{87}Sr/^{86}Sr(t)$	0.752922	0.723202	0.711506				
$^{147}Sm/^{144}Nd$	0.14290	0.12027	0.10448				
$^{143}Nd/^{144}Nd(t)$	0.51189	0.51189	0.51194				
εNd(0)	-10.0	-10.6	-10.3				
εNd(t)	-8.4	-8.3	-7.4				
T_{DM}	2.2.E+09	1.7.E+09	1.4.E+09				

Sample	**LAO-2**	**LAO-3**	**LAO-4**	**LAO-37A**	**LAO-38**	**LAO-40**	**LP-50-1**
Location	Xiang Khuang	Xiang Khuang	Xiang Khuang	Muang Khoun	Muang Khoun	Muang Khoun	Muang Khoun
Rock type	I-type	I-type	I-type	I-type	I-type	I-type	I-type
	Bt granite	Bt granite	Bt granite	Bi-Hbl granite	Bi-Hbl granite	Bt granite	Gabbro-diorite
Age (mill. y)	254		265	257	256		270
SiO_2	71.44	70.88	68.65	71.16	73.28	76.61	56.26
TiO_2	0.14	0.15	0.42	0.38	0.19	0.08	1.12
Al_2O_3	15.32	15.38	14.94	14.20	14.04	12.48	16.56
Fe_2O_3	2.65	2.76	3.25	3.01	1.90	1.16	7.01
MnO	0.06	0.06	0.05	0.06	0.05	0.02	0.14

MgO	0.32	0.41	1.24	0.62	0.26	0.02	5.06
CaO	2.42	2.38	1.76	1.65	1.06	0.49	6.54
Na_2O	3.74	3.94	3.08	3.41	3.76	3.83	3.87
K_2O	3.36	3.31	4.05	5.05	4.87	4.32	1.75
P_2O_5	0.06	0.04	0.12	0.07	0.04	0.02	0.34
LOI	0.95	0.78	2.34	0.76	0.74	0.46	1.16
Total	100.46	100.09	99.89	100.37	100.19	99.49	99.81
Rb*	159.1	178.0	185.0	174.7	225.3	265.0	67.0
Sr*	139.0	135.0	214.0	97.0	72.0	11.1	437.0
Ba	823.0	738.0	401.0	1052.0	504.0	151.0	509.0
Zr*	121.0	130.0	156.0	294.0	177.0	148.0	235.0
Hf	4.0	2.3	1.7	8.9	6.8	3.1	1.2
Nb	7.9	7.5	11.4	18.8	20.7	27.8	12.8
Ta	0.9	1.6	2.1	1.8	2.0	1.9	1.0
Sc	5.0			8.0	2.0	6.0	16.6
Y*	29.7	27.0	38.0	54.7	58.8	95.0	25.5
La	29.8	32.9	33.2	87.6	45.8	15.9	40.1
Ce	60.2	66.0	68.0	140.7	85.6	38.7	75.7
Pr	7.0	7.5	7.7	16.8	10.0	5.5	8.2
Nd	26.0	28.8	29.3	56.2	35.0	23.7	29.4
Sm	5.6	5.8	6.3	10.4	7.8	8.2	5.3
Eu	1.1	1.1	1.0	1.2	0.6	0.1	1.6
Gd	5.3	5.4	6.6	9.9	8.1	10.0	5.6
Tb	0.8	0.6	1.0	1.5	1.4	1.8	0.8
Dy	4.7	3.3	5.6	9.4	8.9	12.0	4.4
Ho	0.9	0.6	1.1	2.0	2.0	2.5	0.9
Er	2.6	1.5	3.1	5.5	5.7	7.4	2.5
Tm	0.4	0.2	0.5	0.9	0.9	1.1	0.4
Yb	2.5	1.3	2.9	5.5	5.9	6.9	2.4
Lu	0.4	0.2	0.4	0.8	0.9	1.0	0.4
V	15.1	9.8	64.0	24.5	16.5	1.4	108.9
Cr	7.0	1.6	18.2	16.0	8.0	2.1	50.9
Co	1.6	2.0	5.7	4.0	2.0	0.4	18.1
Ni	2.0	1.1	6.8	6.0	2.0	0.7	20.2
Cu	2.0	1.9	4.1	2.0	3.0	3.0	-
Zn	34.0	36.4	52.5	44.0	43.0	40.8	-
Pb	24.0	24.1	33.3	13.0	32.0	30.1	8.0
Ga	18.5	17.9	17.7	19.9	21.0	20.7	-
Th	15.1	14.7	16.6	29.9	34.7	33.8	8.8
U	4.4	3.0	5.8	4.9	7.5	8.0	1.6
$^{87}Sr/^{86}Sr$	0.722697	0.723499	0.720327				0.706948
±2s	0.000008	0.000010	0.000007				0.000007
$^{143}Nd/^{144}Nd$	0.512089	0.512103	0.512075				0.512427
±2σ	0.000009	0.000008	0.000009				0.000008
$^{87}Rb/^{86}Sr$	3.193	3.679	2.412				0.428
$^{87}Sr/^{86}Sr(t)$	0.720095	0.720894	0.717734				0.704243
$^{147}Sm/^{144}Nd$	0.13302	0.12474	0.13317				0.11150
$^{143}Nd/^{144}Nd(t)$	0.51187	0.51190	0.51185				0.51224
εNd(0)	-10.7	-10.4	-11.0				-4.1
εNd(t)	-8.7	-8.2	-9.0				-1.5
T_{DM}	2.0.E+09	1.8.E+09	2.0.E+09				1.1.E+09

Sample	LP-50-2-1	LAO-41	LAO-43A
Location	Muang Khoun	Muang Khoun	Muang Khoun
Rock type	I-type	S-type	S-type
	Diorite	Grt-Bt granite	Bt granite
Age (mill. y)	271		253
SiO_2	68.49	68.06	68.30
TiO_2	0.44	0.67	0.66
Al_2O_3	15.14	14.49	13.77
Fe_2O_3	3.23	4.73	4.82
MnO	0.07	0.06	0.06
MgO	1.03	1.40	1.49
CaO	2.7	2.40	2.39
Na_2O	4.44	2.59	2.46
K_2O	3.53	3.78	4.28
P_2O_5	0.13	0.19	0.18
LOI	0.56	0.97	1.56
Total	99.69	99.34	99.99
Rb*	87.0	192.0	187.0
Sr*	232.0	159.0	136.0
Ba	1287.0	638.0	579.0
Zr*	286.0	270.0	262.0
Hf	1.8	0.4	0.6
Nb	13.6	15.6	15.3
Ta	0.9	2.0	2.1
Sc	6.2	20.0	25.0
Y*	22.1	32.0	45.0
La	59.7	41.2	45.2
Ce	103.6	81.6	91.6
Pr	10.3	9.3	10.5
Nd	32.9	34.9	39.2
Sm	5.2	6.7	8.0
Eu	1.4	1.3	1.1
Gd	5.4	6.5	8.1
Tb	0.7	0.8	1.2
Dy	3.8	4.2	6.7
Ho	0.8	0.8	1.3
Er	2.1	1.9	3.7
Tm	0.3	0.3	0.5
Yb	2.0	1.4	3.1
Lu	0.3	0.2	0.5
V	20.2	64.0	67.4
Cr	6.9	27.6	26.7
Co	4.0	9.8	9.5
Ni	2.5	14.1	11.5
Cu	-	19.8	12.5
Zn	-	78.8	69.5
Pb	14.4	25.1	28.7
Ga	-	19.5	17.9
Th	15.6	19.1	23.9
U	1.7	5.2	4.3
$^{87}Sr/^{86}Sr$	0.709614	0.725406	0.724744
±2s	0.000010	0.000010	0.000012
$^{143}Nd/^{144}Nd$	0.512361	0.512153	0.512157
±2σ	0.000010	0.000001	0.000010
$^{87}Rb/^{86}Sr$	1.046	3.369	3.836
$^{87}Sr/^{86}Sr(t)$	0.706898	0.722794	0.722135
$^{147}Sm/^{144}Nd$	0.09795	0.11921	0.12596
$^{143}Nd/^{144}Nd(t)$	0.51220	0.51195	0.51195
εNd(0)	-5.4	-9.5	-9.4
εNd(t)	-2.3	-7.1	-7.2
T_{DM}	1.0.E+09	1.6.E+09	1.7.E+09

Remarks:

$^{87}Sr/^{86}Sr_t = (^{87}Sr/^{86}Sr)_{sample} \times EXP(-\lambda^{87}Rb \times t)$

Where t = 250; $\lambda^{87}Rb = 1.42 \times 10^{-11}$/year

$\varepsilon Nd_{(0)} = ((^{143}Nd/^{144}Nd)_{sample}/CHUR_{(present)})-1) \times 10{,}000)$; $^{143}Nd/^{144}Nd$ of present CHUR is 0.512638

$^{143}Nd/^{144}Nd_{(t)} = ((-^{147}Sm/^{144}Nd_{sample}) \times (2.7183(\lambda^{147}Sm \times t \times 10^6)-1) + {}^{143}Nd/^{144}Nd_{sample})$

t = 250, $\lambda^{147}Sm = 6.54 \times 10^{-12}$/year

$\varepsilon Nd_{(t)} = ((^{143}Nd/^{144}Nd_{(t)}/CHUR_{(t)}) -1 \times 10{,}000)$; CHUR at 250 Ma is 0.512316

$T_{DM} = Ln(((DM_{(present)} - {}^{143}Nd/^{144}Nd_{sample})/({}^{147}Sm/^{144}Nd_{CHUR(t)} - {}^{147}Sm/^{144}Nd_{sample})) + 1 \times 1/\lambda^{147}Sm)$

$DM_{(present)}$ is 0.51315, $^{147}Sm/^{144}Nd_{CHUR(t)}$ is 0.2137, $\lambda^{147}Sm$ is 6.54×10^{-12}/year

(*) analyzed by XRF from pressed samples

5. Analytical results

5.1. Zircon U-Pb ages and Hf isotopic data

Sixteen zircon samples from SN, NP, KC, XK, and MK granitoids were dated by U-Pb, with Hf isotopic analyses on five samples. The U-Pb isotopic data are summarized in Supplementary A (*) and plotted in Fig. 3. At the same time, Hf isotope results are given in Supplementary B (*). Weighted-average ages were calculated from 206Pb/238U for zircons younger than 1000 Ma and from $^{207}Pb/^{206}Pb$ for older detrital cores. Age uncertainties are reported at 2σ. Crustal model ages (T_{DM}) were calculated assuming an average crustal $^{176}Lu/^{177}Hf$ of 0.015 (Griffin et al., 2002).

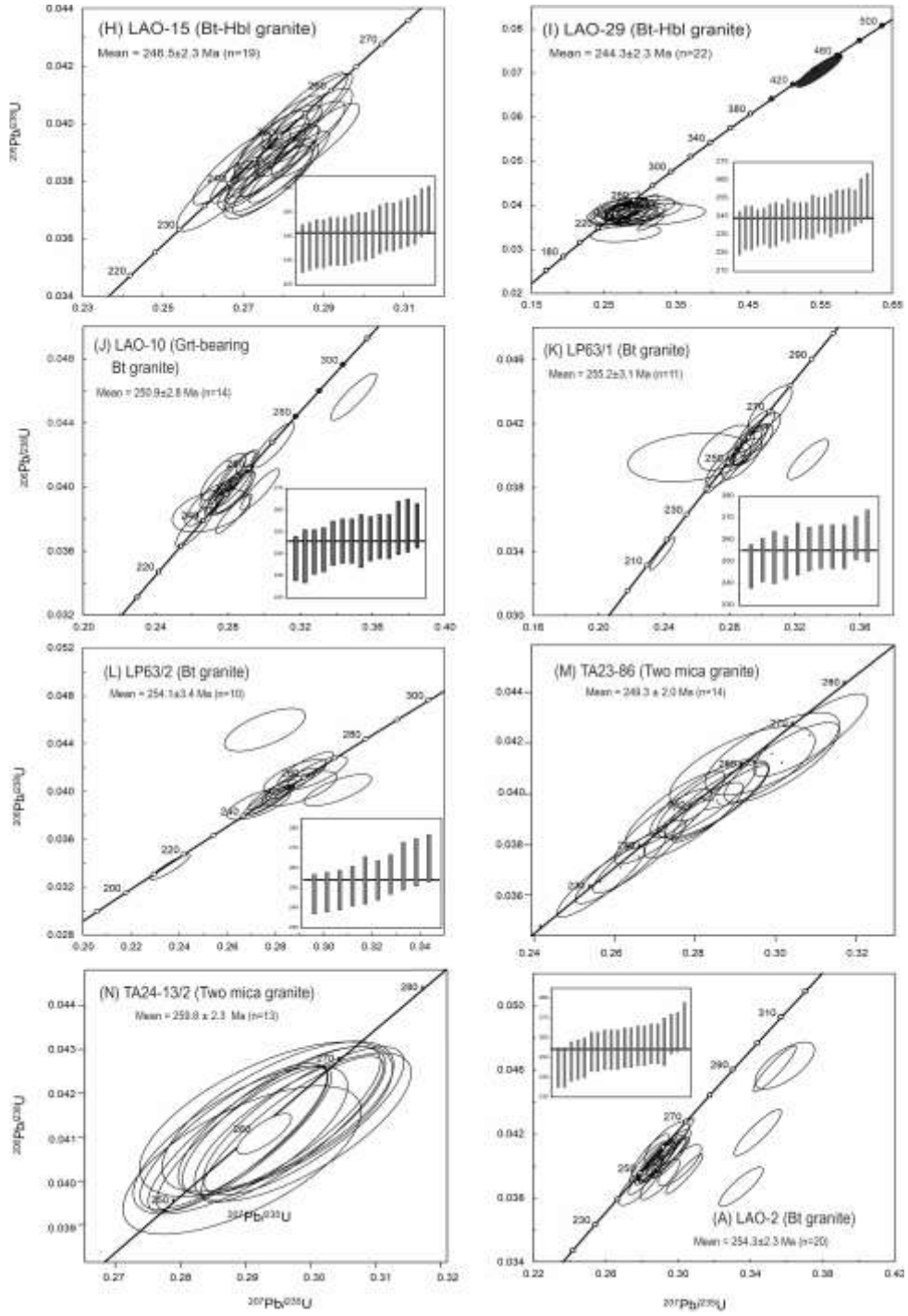

Figure 3. Concordia plots for the Permian-Triassic magmas from northern Laos and western Vietnam

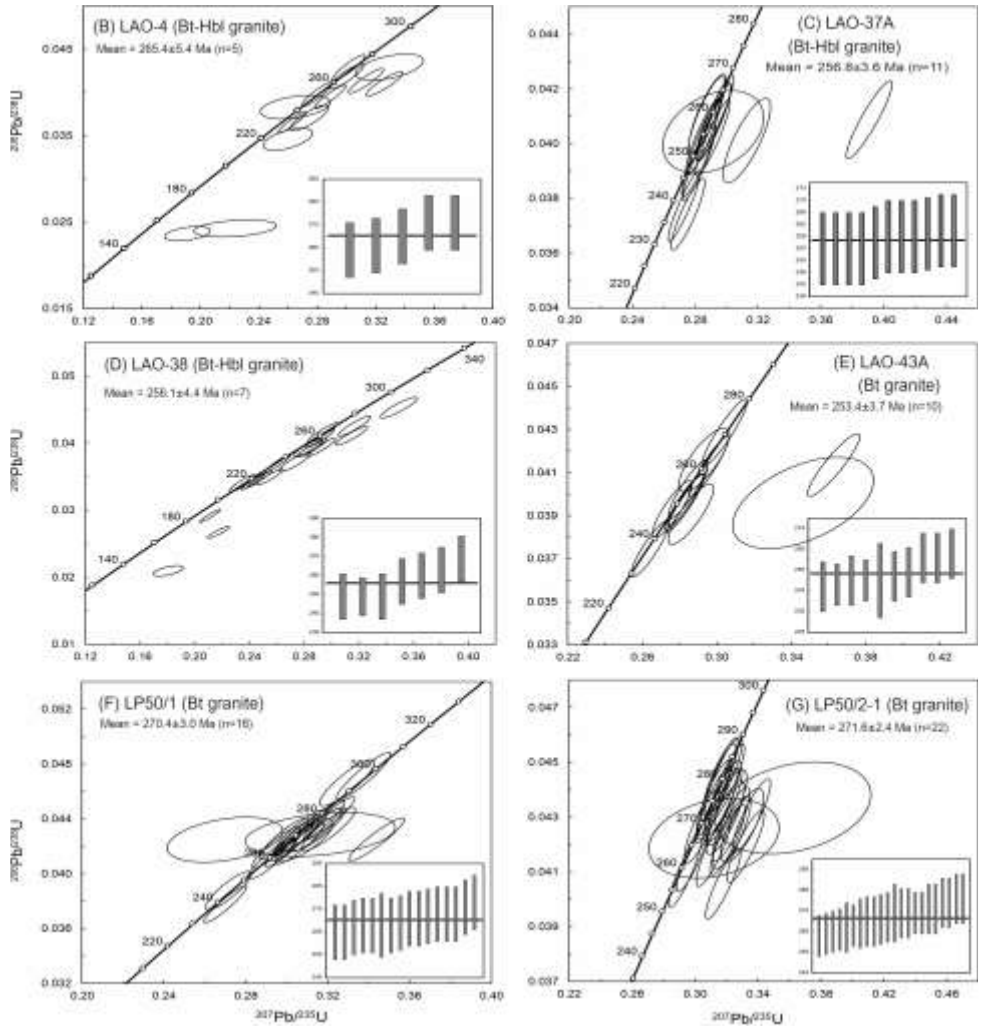

Figure 3. Cont.

5.1.1. Sam Neua (SN) granitoids

Hornblende granites (LAO-15, LAO-29) contain zircons 90–190 μm long with oscillatory rims and sector cores. U contents are 140–790 ppm (Th/U = 1.0–3.0). Weighted average ages are 247 ± 2 Ma (n = 19) and 244 ± 2 Ma (n = 22). εHf(t) values vary from -8.6 to -1.4 and from -7.5 to -2.0, corresponding to T_{DM} ages of 1.4–1.8 Ga.

Garnet-bearing granite (LAO-10) zircons are 110–290 μm long, characterized by oscillatory zoning and occasional detrital cores. Magmatic domains (U = 130–340 ppm; Th/U = 0.4–1.3) give 251 ± 3 Ma (n = 14). Detrital cores range from 407 Ma to 3469 Ma. εHf(t) values of Permian domains are highly variable (-44.8 to -8.2; T_{DM} = 4.1–1.8 Ga). Detrital cores also span a wide range (-33.9 to +15.9; 3.5–1.8 Ga).

5.1.2. Nam Phao (NP) and Kim Cuong (KC) granitoids

Muscovite-bearing granites (LP-63/1, LP-63/2) contain zircons 190–420 μm long with sector cores, oscillatory rims, and detrital cores. Uranium concentrations are 50–1300 ppm (with Th/U = 0.29–3.18), but dark domains are enriched in U (1310–2730 ppm) with very low Th/U (0.03–0.05). Ages are 255 ± 3 Ma (n = 11) and 254 ± 3 Ma

(n = 10). Detrital cores span 340–3458 Ma, while dark domains yield younger ages (214–215 Ma).

Two-mica granites (TA23-86, TA24-13/2) contain zircons 210–430 μm long, with uranium concentrations up to 5125 ppm with low Th/U (0.1–0.75). Ages are 249.3 ± 2.0 Ma (n = 14) and 259.8 ± 2.3 Ma (n = 13).

Summary, granitoids from Xieng Khuang and Muang Khoun record crystallization ages of 265–253 Ma. The Nam Phao and Kim Cuong batholiths, located at similar distances from the Song Ma Suture, also yield ages of 260–249 Ma. Sam Neua granitoids, together with nearby Song Ma intrusions (Tran et al., 2022), are younger (247–227 Ma).

5.1.3. Xieng Khuang (XK) granitoids

Zircons from hornblende granite (LAO-2) and granodiorite (LAO-4) are 90–300 μm long, with aspect ratios from 1.4 to 5.3. LAO-2 exhibits oscillatory or sector zoning, whereas LAO-4 typically features dark rims and detrital cores. U contents range 90–1410 ppm (Th/U = 0.45–2.2), with some dark domains in LAO-4 reaching up to 5440 ppm. Oscillatory domains yield ages of 254 ± 2 Ma (n = 20) and 265 ± 5 Ma (n = 5) for LAO-2 and LAO-4, respectively. Detrital cores range from Paleozoic to Archean, while dark domains give younger ages (151–235 Ma), likely due to hydrothermal modification. εHf(t) values of Permian-Triassic zircons range between +0.4 and -6.4, with T_{DM} ages of 1.3–1.7 Ga; detrital cores range more widely (+9.2 to -10.3; 1.2–2.2 Ga).

5.1.4. Muang Khoun (MK) granitoids

Hornblende granites (LAO-37A, LAO-38) contain zircons 90–170 μm long with oscillatory rims and sector cores. U contents range 310–1780 ppm (Th/U = 0.4–3.9). Weighted average ages are 256.8 ± 3.6 Ma (n = 11) and 256.1 ± 4.4 Ma (n = 7). One detrital core shows an age of 964 Ma; the dark domains, in contrast, give ages of 130–236 Ma.

Biotite granite (LAO-43A) zircons are 130–150 μm long, with magmatic domains showing 160–1080 ppm U (Th/U = 0.41–3.0). A coherent age of 253 ± 4 Ma (n = 10) was obtained, while four detrital cores range from 929 to 1956 Ma.

Quartz diorite (LP-50/1) and granodiorite (LP-50/2-1) zircons (120–240 μm) yield ages of 270.4 ± 3.0 Ma (n = 16) and 271.6 ± 2.4 Ma (n = 22). Detrital cores range 737–2055 Ma.

5.2. Major and trace element results

The granitoids are grouped by locality. Xieng Khuang and Muang Khoun, with similar ages and proximity, are treated as the XK-MK plutons (Fig. 1). Nam Phao and Kim Cuong, spanning the Laos-Vietnam border, are described as a single batholith. The younger Sam Neua granitoids (245–247 Ma), together with nearby Triassic intrusions in the Song Ma Suture in Vietnam (Tran et al., 2022) and Bu Rinh I-type mica granites (242–240 Ma), form a Triassic intrusive group (Fig. 1).

5.2.1. Major element characteristics

XK–MK samples span a wide range of SiO_2 (56–78 wt.%) and Na_2O+K_2O (5–8.3 wt.%), plotting mainly in the granite-granodiorite fields, with a few in quartz monzonite (Fig. 4). A single low-SiO2 sample (LAO-50-1; 56.3 wt.% SiO_2, 5 wt.% Na_2O+K_2O) falls in the gabbro–diorite field. Sam Neua granitoids (63–77 wt.% SiO_2, Na_2O+K_2O = 3–11 wt.%) plot between granodiorite and granite fields. NP-KC biotite granites (63–73 wt.% SiO2) lie mainly in granodiorite. Most granitoids are of the high potassic calc-alkaline series (K_2O = 2.5–4.8 wt.%), with Triassic Sam Neua granitoids plotting in the calc-alkaline field, while two NP–KC samples extend into shoshonite (Fig. 5).

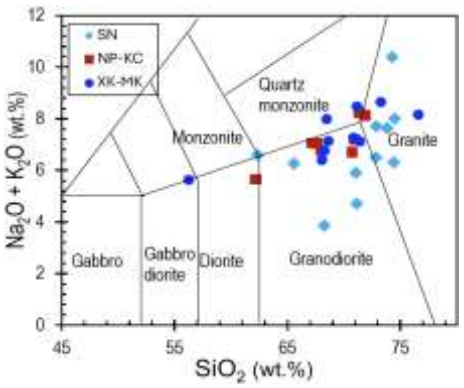

Figure 4. TAS (Na_2O+K_2O vs. SiO_2) diagram (after Middlemost, 1994) of the Permian-Triassic granitoids from the SN, and NP-KC, and XK-MK areas in northern Laos and western Vietnam

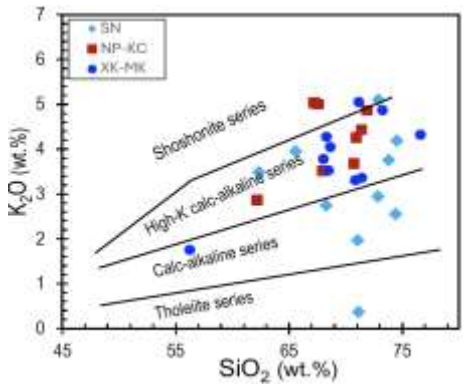

Figure 5. K_2O-SiO_2 classification plot (e.g., Peccerillo and Taylor, 1976) for Permian-Triassic magmatic rocks from the SN, NP-KC, and MK-XK areas in northern Laos and western Vietnam

Across all groups, felsic magmas show reverse correlations between SiO_2 and CaO, Al_2O_3, Fe_2O_3 and MgO (Fig. 6), suggesting fractional crystallization of hornblende/orthopyroxene, feldspar, plagioclase, and mica.

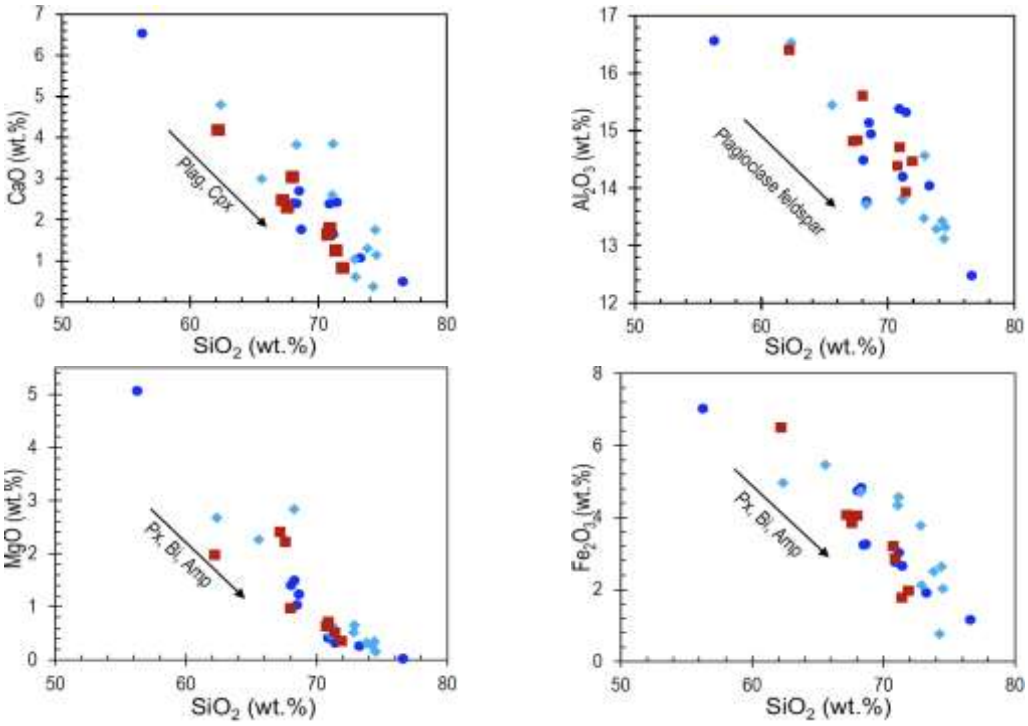

Figure 6. The correlation of (wt.%) SiO_2 versus (wt.%) CaO, Al_2O_3, Fe_2O_3, and MgO for the Permian-Triassic magmas from the SN, NP-KC, and XK-MK areas in northern Laos and western Vietnam. Arrows indicate fractional crystallization of plagioclase (Pl), alkali feldspars (A-Fsp), biotite (Bi), amphibole (Amp), or pyroxene (Px)

Alumina saturation ratios (Maniar and Piccoli, 1989) show most XK-MK granitoids are metaluminous I-type (A/NK = 1.5–3; A/CNK = 0.9–1.1). NP–KC granitoids are mainly metaluminous I-type, though a few plot in peraluminous S-type fields. Sam Neua and nearby Triassic granitoids (A/NK = 1.4–3.5; A/CNK = 0.8–1.3) primarily fall within the peraluminous field (Fig. 7).

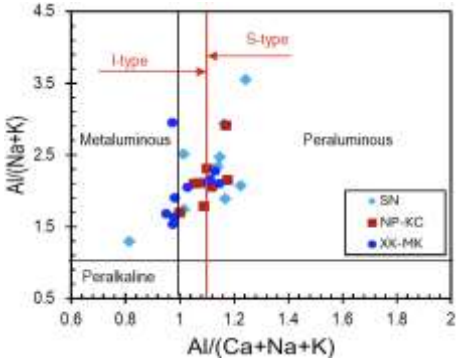

Figure 7. Al/Na+K vs. Al/Ca+Na+K diagram (e.g., Maniar and Piccoli, 1989) for the Permian-Triassic magmatic rocks from the SN, NP-KC, and XK-MK areas in northern Laos and western Vietnam

5.2.2. Trace element characteristics

In 1000Ga/Al vs. Zr and Zr+Nb+Ce+Y discrimination diagrams (Whalen et al. (1987), several XK-MK samples plot in the A-type field (1000Ga/Al > 2.5; Zr > 250 ppm; Zr+Nb+Ce+Y > 350 ppm), while most NP-KC, SN, and some XK–MK samples fall in mixed I- and S-type fields (Figs. 8a-b).

Primitive-mantle normalized trace-element patterns are similar across groups, with negative Nb, Ta, Sr, P, Ti (and locally Hf) anomalies, and positive Th, U, Pb peaks (Fig. 9). Chondrite-normalized REE patterns are also consistent: high in LREE, smooth decrease to heavy REE, slight negative anomalies at Eu, with ratios of $[La/Sm]_N$ from 3 to 4, and $[La/Yb]_N$ between 5 and 17 (up to 21–22 in some MK samples, e.g., LP-50-2-1, LAO-41; Table 1).

5.2.3. Sr-Nd isotopic characteristics

Initial Sr-Nd isotopes (at t = 250 Ma) show enriched signatures. Most XK-MK granitoids have ($^{87}Sr/^{86}Sr$)i = 0.718–0.722, except two older MK samples (ca. 270 Ma; LP-50-1, LP-50-2-1) with lower ratios (0.704–0.707). Their εNdi values range from -4 to -11, forming two isotopic groups (Fig. 10).

The Sam Neua granitoids are the most enriched, with ($^{87}Sr/^{86}Sr$)i ratios ranging from 0.708 to 0.756 and εNdi values of -7 to -14. NP-KC granitoids show narrower variation: ($^{87}Sr/^{86}Sr$)i = 0.71–0.73, εNdi = -7.3 to -9.

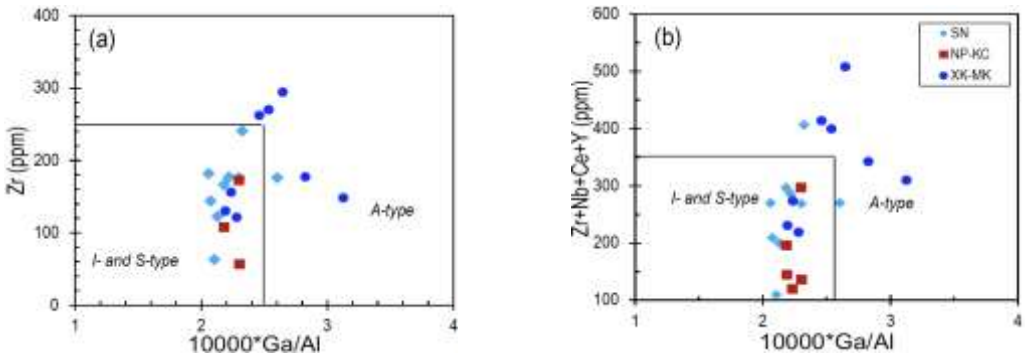

Figure 8. The granitoid type affinity discrimination diagrams (Whalen et al., 1987) for the Permian-Triassic felsic magmas from the TSFB. (a) Zr (ppm) vs. 10000×Ga/Al diagram, and (b) Zr+Nb+Ce+Y (ppm) vs. 10000×Ga/Al diagrams. See descriptions in the text

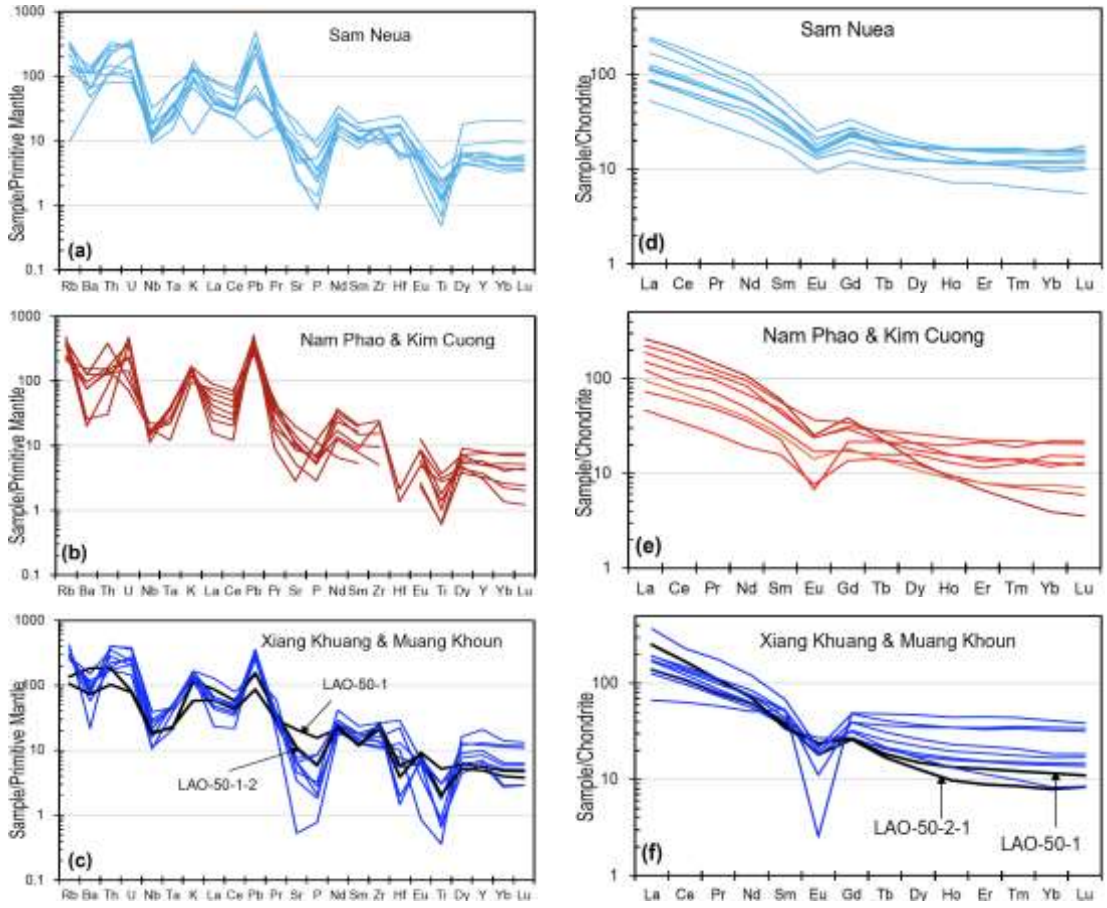

Figure 9. Primitive mantle and chondrite normalization of trace and rare earth elements (REE) (after Sun and McDonough, 1989) for the Permian-Triassic magmas in the TSFB; (a and d), (b and e), and (c and f) are, respectively, for Sam Neua, Nam Phao-Kim Cuong, and Xiang Khuang-Muong Khoun felsic magmatic rocks. See explanations in the text

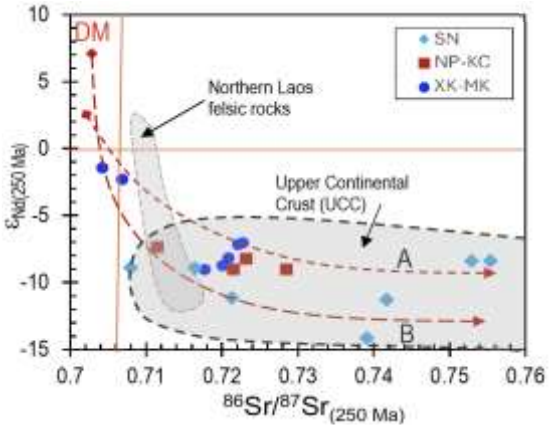

←*Figure 10*. The correlation of $\varepsilon Nd_{(t)}$ vs $^{87}Sr/^{86}Sr_{(t)}$ plots magmatic rocks from the SN, NP-KC, and MK-XK areas in northern Laos and western Vietnam. Mixing curves, A and B, are hypothesized for a depleted source (DM) mixed with a crustal material, resulting in isotopic compositions that depend on the participating portions in the mixing process. The field of the Northern Laos felsic rocks, e.g., Sam Neua and its neighboring areas, is from Qian et al. (2019). Data for Thanh Hoa and Song Ma granitoids are from Tran et al. (2022)

6. Discussions

6.1. Geochronology and tectono-magmatic evolution

Qian et al. (2019) divided the magmatic rocks of northern Laos into four groups: (1) Early Permian (281–276 Ma) high-K, I-type hornblende granodiorite-granites; (2) 274–258 Ma high-K biotite granites with transitional I-S affinities; (3) ca. 261 Ma I-type felsic rocks; and (4) Late Triassic (234–221 Ma) I-type granitoids. Our results, however, show broader age ranges. Hornblende-bearing I-type granitoids span 272–244 Ma, and biotite granites (and felsic volcanics) cluster at 257–251 Ma, significantly younger than those reported by Qian et al. (2019).

This overlap makes classification by rock type problematic. Instead, the data suggest a temporal migration: Early Permian-Triassic granitoids (271–255 Ma) are most prominent in Xieng Khuang-Muang Khoun (XK-MK), while younger intrusions (250–240 Ma) dominate in SN area, adjacent to the Song Ma suture (Fig. 3). Earlier subduction-related magmatism (~300–280 Ma) is also recognized north and south of the study area (Kamvong et al., 2014; Manaka et al., 2014; Hou et al., 2019; Pham et al., 2000; Tran et al., 2022, 2024). This trend indicates progressive migration of igneous activity from arc interior to the suture, consistent with collision of the Indochina and South China blocks at ~250–240 Ma (Lepvrier et al., 2004, 2008; Tran et al., 2008; Cai and Zhang, 2009; Liu et al., 2012; Faure et al., 2014; Pham et al., 2017, 2019; Wang et al., 2016; Qian et al., 2019; Doan et al., 2021; Ngo et al., 2024). We therefore interpret the XK-MK and NP-KC granitoids as pre-collisional (subduction-related), and the 253–240 Ma SN intrusions as collisional to post-collisional.

6.2. Geochemical and isotopic variations

Trace-element patterns of all studied granitoids show reverse Nb, Ta, Ti, and Hf anomalies and positive Th, U, and Pb anomalies (Figs. 9a-c), consistent with crustal melting or subduction-related fluid influence (McLennan, 2001; Rudnick and Gao, 2003; Woodhead et al., 1998; Tatsumi and Eggins, 1995). Overall, XK-MK, NP-KC, and SN granitoids display nearly identical trace-element patterns, suggesting common source characteristics.

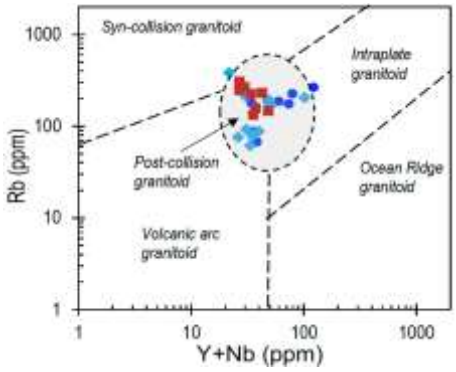

Figure 11. Plots of Rb versus Nb+Y (Pearce et al., 1984; Pearce, 1996) for the SN, NP-KC, and XK-MK magmatic rocks in the TSFB. Redrawn after Ngo et al. (2025). All the granitoids fall in the post-collision field rather than spreading to A, I-, or S-types

Tectonic discrimination based on Y-Nb-Rb (Pearce, 1996; Pearce et al., 1984; Ngo et al., 2025) groups all samples in the post-collision field (Fig. 11). Subtle regional differences exist. Many XK–MK granitoids plot as A-type. NP–KC granitoids fall between I- and S-type with moderate peraluminosity. SN Triassic granitoids are dominantly peraluminous S-type (Fig. 9a–b). This is unlike the East Junggar orogen, where A-type magmas postdate calc-alkaline intrusions (Huang et al., 2023a). The oldest XK–MK granitoids (ca. 255 Ma) already show A-type affinities. This suggests they were generated from sources other than remelting of calc-alkaline rocks. Ce/Pb ratios and absolute Ce contents place most samples between upper continental crust and arc magma fields (Fig. 12). This suggests possible interactions between the sources (Woodhead et al., 1998).

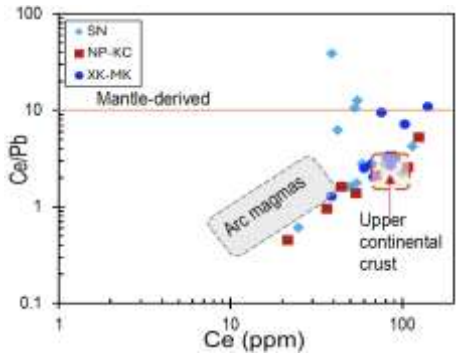

Figure 12. Correlation between Ce (ppm) and Ce/Pb differentiating fields of mantle and crust-derived and arc-related magmatic rocks. Data for the Upper Continental crust are from Rudnick and Gao (2003), arc magmas are from Woodhead et al. (1998)

Sr-Nd isotopes further highlight this trend. Most granitoids are enriched, except for two older Muang Khoun samples (270–271 Ma) with relatively depleted signatures, suggesting mantle input. XK-MK granites have $^{87}Sr/^{86}Sr_t$ from 0.704 to 0.723 and εNd_t ranging between -1.5 and -9, more depleted than NP-KC biotite and two-mica granites (0.712–0.729; εNdi = -7.4 to -9). The SN granitoids are the most enriched, with $^{87}Sr/^{86}Sr_t$ ratios ranging between 0.708 and 0.775 and εNd_t from -8 to to -14 (Fig. 10).

The isotopically most depleted sample is a XK-MK gabbro-diorite $^{87}Sr/^{86}Sr_t$ of 0.7042, and εNd_t of -1.45, T_{DM} ranging between 1.0 and 1.1 Ga. The most enriched is a SN biotite granite $^{87}Sr/^{86}Sr_t$ of 0.775 and εNd_t of -13.8. For example, a XK biotite granite (LAO-2, 254 Ma) yields Nd T_{DM} = 1.6–1.7 Ga and zircon Hf T_{DM} = 1.3–1.7 Ga. The SN biotite-hornblende granites (251–246 Ma) yield εNdi = -9 to -11 and Nd/Hf T_{DM} = 1.5–1.8 Ga. Except for the MK outliers, most samples plot in the enriched upper continental crust field (McDermott and Hawkesworth, 1990; White et al., 2010; Desem et al., 2025).

6.3. Petrogenesis of granitoids in the TSFB

Previous studies showed that granitoids in the TSFB resulted either by (1) mixing of mantle magmas with crustal rocks (Hou et al., 2019), or (2) partial melts of crustal rocks (Qian et al., 2019). Our data support both processes. The relatively depleted gabbro-diorite and granodiorite found in the subduction-related XK-MK batholith point to a mantle contribution. These depleted magmas suggest the existence of a mafic endmember even more primitive than the gabbro-diorite itself. In a binary mixing system, the two endmembers must plot beyond the values of their mixing products (Carlson and Irving, 1994). Thus, the isotopic arrays for individual magma batches in XK-MK, NP-KC, and SN (Fig. 10) likely reflect different proportions and degrees of heterogeneity in their mantle and crustal endmembers.

For the XK-MK and NP-KC granitoids, mixing between a relatively mafic melt (with $^{87}Sr/^{86}Sr \approx 0.7045$ and $\varepsilon Nd \approx +3$) and a crustal melt ($^{87}Sr/^{86}Sr \approx 0.730$ and $\varepsilon Nd \approx -9$) could explain the observed isotopic characteristics. In addition, the reverse correlations of SiO_2 versus CaO, Al_2O_3, Fe_2O_3, and MgO (Fig. 6) suggest fractionation of plagioclase feldspar, pyroxene, biotite, and amphibole, along with crustal material assimilation. The low-SiO_2, low-$^{87}Sr/^{86}Sr$ gabbro-diorite from MK (e.g., LP-50-1) likely represents one mantle-derived endmember.

In contrast, the SN granitoids show no clear correlation among major oxides and display high $^{87}Sr/^{86}Sr$ ratios and low εNd values. These features suggest a dominant crustal melting origin, with little to no mantle input (Fig. 10).

Zircon U-Pb ages further constrain these processes. The XK-MK granitoids (271–254 Ma) largely overlap with those of NP-KC (260–254 Ma), both of which were emplaced relatively far from the Song Ma Suture. Their timing coincides with ongoing subduction of Paleotethys under the Indochina between ~280 and 250 Ma (Lan et al., 2000; Lepvrier et al., 2008; Tran et al., 2008). Other studies propose more detailed tectono-magmatic

stages: subduction (280–245 Ma), syn-collision (245–230 Ma), and post-collision (230–200 Ma) (Liu et al., 2012; Qian et al., 2019; Hou et al., 2019; Luong et al., 2024). Accordingly, the SN granitoids of 246–227 Ma fall into the syn- to post-collisional stages (Tran et al., 2008; Liu et al., 2012).

6.4. Geological implications

Based on the granitoids' geochronologic, geochemical, and isotopic variations from this study, together with previous work, the tectonic evolution of the TSFB may be outlined as follows:

(a) Pre-collision (subduction) stage

Southward subduction of the Paleotethys under the Indochina Block began at ~306–304 Ma (Kamvong et al., 2014) and lasted until ~250 Ma. Evidence for this comes from Permian–Triassic igneous rocks in north-central Vietnam (Tran et al., 2008; Liu et al., 2012) and northern Laos (Qian et al., 2019). The granitoids in the XK-MK and NP-KC areas, dated between ~270 and 250 Ma, are consistent with this stage. Their arc-like geochemistry and isotope characteristics may be explained by the mixing of mantle mafic magmas with crustal melts. The crustal contributions likely originated from the melting of both ancient (1.6–1.9 Ga) and younger (~1 Ga) basement rocks, triggered by the underplating of mafic magmas (e.g., Gao et al., 2014).

(b) Syn-collision stage

Most researchers agree that a collision between the South China and Indochina blocks occurred between 250 and 243 Ma (Lepvrier et al., 2004, 2008; Tran et al., 2008; Cai and Zhang, 2009; Liu et al., 2012; Faure et al., 2014, 2018; Pham et al., 2017, 2019; Pham et al., 2023; Wang et al., 2016; Qian et al., 2019). In the SN area, zircon U-Pb ages of felsic magmas range from 253 to 240 Ma, matching this timeframe. Numerical models (Magni et al., 2012) indicate that once continental collision commences, the subducting slab stalls and rollback occurs, thereby shifting magmatism closer to the trench. A similar process was proposed for syn-collision granites in the Tanggula batholith of northern Qiantang (Song et al., 2022). In the TSB, slab rollback could explain why felsic magmatism migrated from inland areas (XK-MK, NP-KC) toward the suture-proximal SN area (e.g., Huang et al., 2023b). The incorporation of 1.9 Ga or older crustal material into the 250–240 Ma SN granites suggest input from the ancient South China margin (Lan et al., 2000; Tran et al., 2024).

(c) Post-collision stage

Although not the focus of this study, post-collisional granitoids (dating back to 235–200 Ma) are recognized across the TSFB (Wang et al., 2016; Qian et al., 2019). For example, diorite and biotite-hornblende granites dated at 230–227 Ma occur in the Song Ma area, just across the suture from the SN batholith (Li et al., 2021). These may represent a continuation of post-collision magmatism in the region (Tran et al., 2022; Luong et al., 2024) (Fig. 1).

7. Conclusions

From zircon U-Pb isotopic ages, magma geochemistry, and Sr-Nd isotopic data of Permian-Triassic granitoids in northern Laos and western Vietnam, the following conclusions may be drawn:

(1) The granitoids in the Sam Neua (SN), Nam Phao-Kim Cuong (NP-KC), and Xieng Khuang–Muong Khoun (XK-MK) areas show arc-related geochemical signatures.

(2) Subduction-related magmatism occurred between ~280–250 Ma in the NP-KC and XK-MK areas. In contrast, magmatism in the SN area, adjacent to the Song Ma Suture zone, took place between 250 and 240 Ma, coinciding with the timing of continental collision between the Indochina and South China blocks.

(3) Sr-Nd isotopic compositions indicate that magmas formed through mixing of mantle mafic components with ancient crustal rocks' melts via assimilation and fractional crystallization. The NP-KC and XK-MK magmas reflect inputs from 1.1–1.2 Ga and 1.6–1.7 Ga crustal sources, whereas the SN felsic magmas were generated mainly from older 1.9–2.2 Ga crustal materials.

(4) The shift of younger magmatism toward the suture zone is best explained by slab rollback during collision. The involvement of 1.9–2.2 Ga components in the SN magmas likely records the incorporation of ancient crust from the subducted South China margin.

Acknowledgments

We thank Prof. S.L. Chung for providing access to chemical laboratories and analytical facilities at the Institute of Earth Sciences, Academia Sinica, and the Department of Geosciences, NTU. We are grateful to M. Usuki and W.Y. Hsu for assistance with Sr and Nd isotope analyses, and to C.H. Hung and H.Y. Lee for zircon U-Pb dating, and zircon Hf isotope measurements. We thank Prof. Daizo Ishiyama of Akita University for providing analytical facilities and assisting with ICP-MS and XRF analysis. We also thank Y.S. Wang and Y. Iizuka for CL imaging of zircon grains at IES, Academia Sinica. Two anonymous reviewers are thanked for valuable suggestions and critical comments.

This study was financed by the Vietnam Ministry of Science and Technology, under grant number DTDLCN.15/23, to whom the authors express their sincere gratitude.

References

Andersen T., 2002. Correction on common Pb in U-Pb analyses that do not report ^{204}Pb. Chemical Geology, 192, 59–79.

Cai J.X., Zhang K.J., 2009. A new model for the Indochina and South China collision during the Late Permian to the Middle Triassic. Tectonophysics, 467(1–4), 35–43. https://doi.org/10.1016/j.tecto.2008.12.003.

Carlson R.W., Irwing A.J., 1994. Depletion and Enrichment History of Subcontinental Lithospheric Mantle: An Os, Sr, Nd and Pb Isotopic Study of Ultramafic Xenoliths from Northwestern Wyoming Craton. Earth and Planetary Science Letters, 126, 209–220. https://doi.org/10.1016/0012-821X(94)90124-4.

Doan D.H., Tsutsumi Y., Pham T.H., Nguyen T.M., Pham M., Nguyen T.D., Nguyen B.H., Komatsu T., Hoang N., Kawaguchi K., 2022. Van Canh Triassic granite in the Kontum Massif, central Vietnam: Geochemistry, geochronology, and tectonic implications. Journal of Asian Earth Sciences, X(7), 100075. https://doi.org/10.1016/j.jaesx.2021.100075.

Desem C.U., Woodhead J., de Caritat P., Maas R., Champion D.C., Dosseto A., Wainwright A., Carr G., 2025. The Pb, Sr and Nd isotopic composition of the upper continental crust: an Australian perspective. Chem. Geol., 672, 122503.

Faure M., Lepvrier C., Nguyen V.V., Vu T.V., Lin W., Chen Z., 2014. The South China block-Indochina collision: where, when, and how. J. Asian Earth Sci., 79(Part A), 260–274. https://doi.org/10.1016/j.jseaes.2013.09.022.

Faure M., Nguyen V.V., Luong T.T.H., Lepvrier C., 2018. Early Paleozoic or Early-Middle Triassic collision between the South China and Indochina Blocks: The controversy resolved? Structural insights from the Kon Tum massif (Central Vietnam). Journal of Asian Earth Sciences, 166, 162–180.

Fukuyama M., Kawamoto T., Ogasawara M., 2017. Chemical composition of fluid inclusions in the Yorii jadeite-quartz rocks from the Kanto Mountains, Japan. Journal of Mineralogical and Petrological Sciences, 112, 281–290. Doi: 10.2465/jmps.170331.

Fukuyama M., Ogasawara M., Horie K., Lee D.C., 2013. Genesis of jadeite-quartz rocks in the Yorii area of the Kanto Mountains, Japan. Journal of Asian Earth Sciences, 63, 206–217. https://doi.org/10.1016/j.jseaes.2012.10.031.

Gao W., Wang Z., Song W., Wang D., Li, C., 2014. Zircon U-Pb geochronology, geochemistry and tectonic implications of Triassic A-type granites from southeastern Zhejiang, South China. Journal of

Asian Earth Sciences, 96, 255–268. https://doi.org/10.1016/j.jseaes.2014.09.024.

Griffin W.L., Wang X., Jackson S.E., Pearson N.J., O'Reilly S.Y., Xu X., Zhou X., 2002. Zircon chemistry and magma mixing, SE China: in-situ analysis of Hf isotopes, Tonglu and Pingtan igneous complexes. Lithos, 61, 237–269. https://doi.org/10.1016/S0024-4937(02)00082-8.

Hou L., Liu S., Guo L., Xiong F., Li C., Shi M., Zhang Q., Xu S., Wu S., 2019. Geology, geochronology, and Hf isotopic composition of the Pha Lek Fe deposit, Northern Laos: implications for Early Permian subduction - related skarn Fe mineralization in the Truong Son Belt. Journal of Earth Sciences, 30(1), 109–120 (Printed in China).

Huang C., Chen B., Sun K., 2023a. A-type granites derived from dehydration melting of calc-alkaline granitoids in East Junggaer (NW China): Implications for the origin of aluminous and peralkaline A-types. Lithos, 440–441, 107043. https://doi.org/10.1016/j.lithos.2023.107043.

Huang W-M., Liu X-L., Liu L., Li Z-L, Liu X., Wu H., 2023b. Early Triassic rollback of subducted Paleotethys oceanic lithosphere: Insights from A2-type silicic igneous rocks in the Pingxiang area, southwest China. Geosphere. https://doi.org/10.1130/GES02617.1.

Jackson S.E., Pearson N.J., Griffin W.L., Belousova E.A., 2004. The application of laser ablation-inductively coupled plasma-mass spectrometry to in situ U-Pb zircon geochronology. Chemical Geology, 211, 47–69. https://doi.org/10.1016/j.chemgeo.2004.06.017.

Jahn B.-M., Litvinovsky B., Zanvilevich A., Reichow M., 2009. Peralkaline granitoid magmatism in the Mongolian-Transbaikalian Belt: evolution, petrogenesis and tectonic significance. Lithos, 113, 521–539. https://doi.org/10.1016/j.lithos.2009.06.015.

Jian P., Liu D., Sun X., 2008. SHRIMP dating of the Permo-Carboniferous Jinshajiang ophiolite, southwestern China: geochronological constraints for the evolution of Paleotethys. Journal of Asian Earth Sciences, 32, 371–384. https://doi.org/10.1016/j.jseaes.2007.11.006.

Kamvong T., Zaw K., Meffre S., Maas R., Stein H., Lai C.K., 2014. Adakites in the Truong Son and Loei fold belts, Thailand and Laos: Genesis and implications for geodynamics and metallogeny. Gondwana Research, 26(1), 165–184. https://doi.org/10.1016/j.gr.2013.06.011.

Lan C.-Y., Chung S.-L., Shen J.J-S., Lo C.-H., Wang P.-L., Tran T.H., Hoang H.T., Mertzman S.A., 2000. Geochemical and Sr-Nd isotopic characteristics of granitic rocks from northern Vietnam. Journal of Asian Earth Sciences, 18, 267–280. https://doi.org/10.1016/S1367-9120(99)00063-2.

Le D.A., Hoang N., Shakirov R.B., Huong T.T., 2017. Geochemistry of late Miocene-Pleistocene basalts in the Phu Quy island area (East Vietnam Sea): Implication for mantle source feature and melt generation. Vietnam Journal of Earth Sciences, 39(3), 270–288. Doi: 10.15625/0866-7187/39/3/10559.

Le D.B., Vu M.Q., Tran Q.H., Ngo G.T., Hoang H.T., 1982. The Song Ma ophiolite. Journal of Earth Sciences. Hanoi, 4(4), 97–106 (in Vietnamese).

Lepvrier C., Maluski H., Vuong N.V., Roques D., Axente V., Rangin C., 1997. Indosinian NW-trending shear zones within the Truong Son belt (Vietnam): Ar-Ar Triassic ages and Cretaceous to Cenozoic overprints. Tectonophysics, 283(1–4), 105–127. https://doi.org/10.1016/S0040-1951(97)00151-0.

Lepvrier C., Maluski, H., Vu V.T., Leyreloup, A., Phan T.T., Nguyen V.V., 2004. The Early Triassic Indosinian orogeny in Vietnam (Truong Son Belt and Kontum Massif); implications for the geodynamic evolution of Indochina. Tectonophysics, 393, 87–118. https://doi.org/10.1016/j.tecto.2004.07.030.

Lepvrier C., Nguyen V.V., Maluski, H., Truong Thi, P., Van Vu, T., 2008. Indosinian tectonics in Vietnam. Comptes Rendus-Geosci, 340, 94–111. https://doi.org/10.1016/j.crte.2007.10.005.

Li Q., Lin W., Wang Y., Faure M., Meng L., Wang H., Nguyen V.V., Luong T.T.H., Lepvrier C., Chu Y., Wei W., Vu V.T., 2021. Detrital zircon U-Pb age distributions and Hf isotopic constraints of the Ailaoshan-Song Ma Suture Zone and their paleogeographic implications for the Eastern Paleo-Tethys evolution. Earth-Science Reviews, 21, 103789. https://doi.org/10.1016/j.earscirev.2021.103789.

Liu J., Tran M.-D., Tang Y., Nguyen Q.-L., Tran T.-H., Wu W., Chen J., Zhang Z., Zhao Z., 2012. Permo-Triassic granitoids in the northern part of the Truong Son belt, NW Vietnam: Geochronology, geochemistry and tectonic implications: Gondwana Research, 22(2), 628–644. https://doi.org/10.1016/j.gr.2011.10.011.

Ludwig K.R., 2008. Isoplot V. 4.15: Geochronol. Toolkit for Microsoft Excel. Spec. Publ. (Berkley Geochronol. Center).

Luong T.T.H., Nguyen V.V., Faure M., Wei L., Vu T.T., Tran T.T.N., Nguyen T.M.T., 2024. From rifting to Indosinia orogeny recorded in the Indochina from late Devonian to late Triassic: a review. Vietnam Journal of Earth Sciences, 47(1), 61–103. https://doi.org/10.15625/2615-7983/21910.

Magni V., Van Hunen J., Funiciello F., Faccenna C., 2012. Numerical models of slab migration in continental collision zones. Solid Earth, 3, 293–306.

Manaka T., Zaw, K., Meffre, S., et al., 2014. The Ban Houayxai Epithermal Au-Ag Deposit in the Northern Lao PDR: Mineralization Related to the Early Permian Arc Magmatism of the Truong Son Fold Belt. Gondwana Research, 26(1), 185–197. https://doi.org/10.1016/j.gr.2013.08.024.

Maniar P.D., Piccoli P.M., 1989. Tectonic discrimination of granitoids. Geol. Soc. Am. Bull., 101, 635–643.

McDermott F., Hawkesworth C., 1990; The evolution of strontium isotopes in the upper continental crust. Nature, 344, 850–853.

McLennan S.M., 2001. Relationships between the Trace Element Composition of Sedimentary Rocks and Upper Continental Crust. Geochemistry, Geophysics, Geosystems, 2. https://doi.org/10.1029/2000GC000109.

Metcalfe I., 2013. Gondwana dispersion and Asian accretion: tectonic and palaeogeographic evolution of eastern Tethys. J. Asian Earth Sci., 66, 1–33. https://doi.org/10.1016/j.jseaes.2012.12.020.

Middlemost E.A.K., 1985. Magma and magmatic rock. Longman, London, p.266.

Ngo T.H., Svetlitskaya T.V., Tran T.A., Izokh A.E., Nevolko P.A., Tran T.H., Vu H.L., Ngo T.P., 2024. Indosinian magmatism in NE Vietnam: Petrogenesis and geodynamic implications of Triassic mafic suites from the Song Hien region. Lithos, 488–489, 107842. https://doi.org/10.1016/j.lithos.2024.107842.

Ngo X.T., Luong Q.K., Bui V.H., Tran T.H., Nguyen Q.H., Dinh T.T., 2025. Petrogenesis and geological significance of the early Paleozoic S-Type granitic mylonite in the Southwestern Kon Tum Massif, Central Vietnam. Vietnam Journal of Earth Sciences, 47(3), 1–18. https://doi.org/10.15625/2615-9783/23115.

Pearce J.A., 1996. Sources and settings of granitic rocks. Episodes, 19, 120–125.

Pearce J.A., Harris, N.W., Tindle A.G., 1984. Trace element discrimination diagrams for the tectonic interpretation of granitic rocks. J. Petrol., 25(4), 956–983. http://dx.doi.org/10.1093/petrology/25.4.956.

Peccerillo A., Taylor S.R., 1976. Geochemistry of Eocene Calc-Alkaline Volcanic Rocks from the Kastamonu Area, Northern Turkey. Contributions to Mineralogy and Petrology, 58, 63–81.

Pham N.C., Tran T-A., Tran T.H., Vu H.L., Pham T.P.L., Ngo T.H., 2020. Chemical compositions of amphiboles and their references to formation conditions of granitoids from Nam Rom and Song Ma massifs, Northwest Vietnam. Vietnam Journal of Earth Sciences, 42(1), 80–92. https://doi.org/10.15625/0866-7187/42/1/14760.

Pham T.D., Usuki T., Tran T.H., Hoang N., Usuki M., Pham M., Nong T.Q.A., Nguyen V.Y., Pham T.H., 2023. Emplacement ages, geochemical and Sr-Nd-Hf isotopic characteristics of Cenozoic granites in the Phan Si Pan uplift, Northwestern Vietnam: petrogenesis and tectonic implication for the adjacent structure of the Red River shear zone. International Journal of Earth Sciences, 112, 1475–1497. https://doi.org/10.1007/s00531-023-02307-4.

Pham T.H., Nong T.Q.A., Pham M., Nguyen T.B.T., 2019. Geochemistry, zircon U-Pb ages and Hf isotopes of Muong Luan granitoid pluton, Northwest Vietnam and petrogenetic significance. Island Arc. Doi: 10.1111/iar.12330.

Pham T.H., Li S.Q., Yang Y., Ngo X.T., Le T.D., Vu L.T., Wolfgang S., Fukun C., 2017. Stages of late Paleozoic to early Mesozoic magmatism in the Song Ma belt, NW Vietnam: evidence from zircon U-Pb geochronology and Hf isotope composition. Int. J. Earth Sci. (Geol Rundsch), 106, 855–874. Doi: 10.1007/s00531-016-1337-9.

Phan C.T. (Editor), 2009. Geological Map of Cambodia, Laos and Vietnam, Scale 1:1.500,000. Vietnam Institute of Geosciences and Mineral Resources (VIGMR) (in Vietnamese).

Qian X., Wang Y., Zhang Y., Zhang Y., Senebouttalath V., Zhang A., He H., 2019. Petrogenesis of Permian-Triassic felsic igneous rocks along the Truong Son zone in northern Laos and their Paleotethyan assembly. Lithos, 328–329, 101–114. https://doi.org/10.1016/j.lithos.2019.01.006.

Rudnick R., Gao S., 2003. Composition of the continental crust. Treatise Geochemistry, 3, 1–64.

Scherer E.E., Münker, C., Mezger, K., 2001. Calibration of the lutetium-hafnium clock. Science, 293, 683–687.

Sláma J., Košler J., Condon D.J., Crowley J.L., Gerdes A., Hanchar J.M., Horstwood M.S.A., Morris G.A., Nasdala L., Norberg N., Schaltegger U., Schoene B., Tubrett M.N., Whitehouse M.J., 2008. Plešovice zircon a new natural reference material for U-Pb and Hf isotopic microanalysis. Chemical Geology, 249, 1–35. https://doi.org/10.1016/j.chemgeo.2007.11.005.

Song S.W., Zhu D.C., Wang Q., Cawood P.A., Zhan Q.Y., Li S.M., Zhang L.L., Zhao Z.D., 2022. Generation of syn-collisional S-type granites in collision zones: An example from the Late Triassic Tanggula Batholith in northern Tibet. Gondwana Res., 104, 185–198. https://doi.org/10.1016/j.gr.2020.12.023.

Sun S.S., McDonough W.F., 1989. Chemical and isotopic systematics of oceanic basalts; implications for mantle composition and processes. In: Magmatism in the ocean basins. Saunders A.D. & Norry M.J. (Eds.), Geological Society of London, London, 42, 313–345.

Tatsumi Y., Eggins, S.M., 1995. Subduction zone magmatism. Blackwell, Cambridge, 211p.

Tran T-A., Pham N.C., Hoang N., Vu H.L., Ngo T.H., Tran Q.C., Pham T.P.L., Tran T.H., Vuong B.T.S., Pham T.T., 2024. Petrological and geochemical characteristics of the Low- and High-Hf Nam Meng dioritoid, northwest Vietnam: Implication for the mantle partial melting, mixing, and magmatic differentiation. Vietnam Journal of Earth Sciences, 46(2), 252–271. https://doi.org/10.15625/2615-9783/20274.

Tran T-A., Tran T.H., Pham N.C., Shellnutt, G.J, Pham T.T., Izokh E.A., Pham T.P.L., Somsanith Duangpaseuth, Oneta Soulintone., 2022. Petrology of the Permian-Triassic granitoids in Northwest Vietnam and their relation to the amalgamation of the Indochina and Sino-Vietnam composite terranes. Vietnam Journal of Earth Sciences, 44(3), 343–368. https://doi.org/10.15625/2615-9783/17002.

Tran T.H., Tran T-A, Ngo T.P., Pham T.D., Tran V.A., Izokh A.E., Borisenko A.S., Lan C.Y., Chung S.L., Lo C.H., 2008. Permo-Triassic intermediate-felsic magmatism of the Truong Son belt, eastern margin of Indochina. C. R. Geoscience, 340, 112–126.

Tran-Van T., 1977. In Geology of Vietnam: Northern part. Sciences and Technics Publishing House, Hanoi, p.355 (in Vietnamese).

Tran-Van, T., Faure M., Nguyen V.V., Bui H.H., Bryl M., Fyhn W., Nguyen Q.T., Lepvrier C., Thomsene B.T., Tani K., Charusiri P., 2020. Neoproterozoic to Early Triassic tectono-stratigraphic evolution of Indochina and adjacent areas: A review with new data. J. Asian Earth Sciences, 191, 104231. https://doi.org/10.1016/j.jseaes.2020.104231.

Tran-Van T., Vu K. (Eds.), 2011. Geology and Earth Resources of Vietnam, 2011th Ed. Vietnam Publish House for Science and Technology, Hanoi, p.646.

Usuki T., Lan C.Y., Wang K.L., Chiu H.Y., 2013. Linking the Indochina block and Gondwana during the Early Paleozoic: Evidence from U-Pb ages and Hf isotopes of detrital zircons. Tectonophysics, 586, 145–159. http://dx.doi.org/10.1016/j.tecto.2012.11.010

Wang S., Mo Y., Wang C., Ye, P., 2016. Paleotethyan evolution of the Indochina Block as deduced from granites in northern Laos. Gondwana Research, 38, 183–196. https://doi.org/10.1016/j.gr.2015.11.011.

Whalen J.B., Currie K.L., Chappell B.W., 1987. A-type granites: geochemical characteristics, discrimination and petrogenesis. Contrib. Miner. Petrol., 95, 407–419.

White W.M., 2010. Oceanic island basalts and mantle plumes: the geochemical perspective. Annual Rev. Earth Planet. Sci., 38(1), 133–160.

Wiedenbeck M.A.P.C., Alle P., Corfu F., Griffin W.L., Meier M., Oberli F., Spiegel W., 1995. Three natural zircon standards for U-Th-Pb, Lu-Hf, trace element and REE analyses. Geostandards Newsletter, 19, 1–23. Doi: 10.1111/j.1751-908X.1995.tb00147.x.

Woodhead J.D., Hergt J.M., 2005, A preliminary appraisal of seven natural zircon reference materials for in situ Hf isotope determination: Geostandards and Geoanalytical Research, 29(2), 183–195.

Woodhead J.D., Eggins S.M., Johnson R.W., 1998. Magma genesis in the New Britain island arc: Further insights into melting and mass transfer processes. Journal of Petrology, 39, 1641–1668. Doi: 10.1093/PETROJ/39.9.1641.

Zhang Zh., Shu Q., Wu Ch., Zaw K., Cromie P., von Dollen M., Xu J., Li X., 2020. The endogenetic metallogeny of northern Laos and its relation to the intermediate-felsic magmatism at different stages of the Paleotethyan tectonics: A review and synthesis. Ore Geology Reviews, 123, 103582. https://doi.org/10.1016/j.oregeorev.2020.103582.